PHYSICAL REVIEW D **83,** 016001 (2011)

Casimir scaling and string breaking in G_2 gluodynamics

Björn H. Wellegehausen,* Andreas Wipf,† and Christian Wozar‡

Theoretisch-Physikalisches Institut, Friedrich-Schiller-Universität Jena, Max-Wien-Platz 1, 07743 Jena, Germany

(Received 20 August 2010; published 4 January 2011)

We study the potential energy between static charges in G_2 gluodynamics in three and four dimensions. Our work is based on an efficient local hybrid Monte Carlo algorithm and a multilevel Lüscher-Weisz algorithm with exponential error reduction to accurately measure expectation values of Wilson and Polyakov loops. Both in three and four dimensions we show that at intermediate scales the string tensions for charges in various G_2 representations scale with the second order Casimir. In three dimensions Casimir scaling is confirmed within 4% for charges in representations of dimensions 7, 14, 27, 64, 77, 77′, 182, and 189 and in four dimensions within 5% for charges in representations of dimensions 7, 14, 27, and 64. In three dimensions we detect string breaking for charges in the two fundamental representations. The scale for string breaking agrees very well with the mass of the created pair of glue lumps. Close to the string breaking distance Casimir scaling between adjoint and defining representation is violated by 2.5%. The analytical prediction for the continuum string tension is confirmed for the defining representation in three dimensions.

DOI: 10.1103/PhysRevD.83.016001 PACS numbers: 11.15.−q, 11.15.Ha, 12.38.Aw

I. INTRODUCTION

There is compelling experimental evidence that the fundamental constituents of QCD, quarks, and gluons, never show up as asymptotic states of strong interaction—rather they are confined in mesons and baryons. Understanding the dynamics of this confinement mechanism is one of the challenging problems in strongly coupled gauge theories. There are convincing analytical and numerical arguments to believe that confinement is a property of pure gauge theories (gluodynamics) alone and that the underlying mechanism should not depend on the number N_c of colors. Confinement is lost at high temperatures and for gauge groups with a nontrivial center the trace of the Polyakov loop

$$\begin{aligned} P(\vec{x}) &= \operatorname{tr} \mathcal{P}(\vec{x}), \\ \mathcal{P}(\vec{x}) &= \frac{1}{N} \operatorname{tr}\left(\exp\, i \int_0^{\beta_T} A_0(\tau, \vec{x}) d\tau\right), \\ \beta_T &= \frac{1}{T}, \end{aligned} \tag{1}$$

vanishes in the confined low-temperature phase and is close to an element of the center in the deconfined high-temperature phase. In gluodynamics or gauge theories with matter in the adjoint representation the action and measure are both invariant under *center transformations*, whereas the Polyakov loop transforms nontrivially and hence serves as order parameter for the global center symmetry. This means that the center symmetry is realized in the confined phase and spontaneously broken in the deconfined phase.

In the vicinity of the transition point the dynamics of the Polyakov loop is successfully described by effective three dimensional scalar field models for the characters of the Polyakov loop [1–4]. If one further projects the scalar fields onto the center of the gauge group then one arrives at generalized Potts models describing the effective Polyakov loop dynamics [5]. The temperature dependent couplings constants of these effective theories have been calculated *ab initio* by inverse Monte Carlo methods in [3].

With dynamical quarks in the fundamental representation the center symmetry is *explicitly broken* and the Polyakov loop points always in the direction of a particular center element. In a strict sense the Polyakov loop ceases to be an order parameter. This is attributed to breaking of the string connecting a static ''quark antiquark pair'' when one tries to separate the charges. It breaks via the spontaneous creation of dynamical quark antiquark pairs which in turn screen the individual static charges.

The pivotal role of the center for confinement also follows from a recent observation relating the Polyakov loop with center averaged spectral sums of the Dirac operator [6–8]. More precisely, for gauge groups with a *nontrivial center* one can relate the expectation value of the Polyakov loop to dual condensates. This result could finally explain why for gauge groups with a nontrivial center and fundamental matter the transition temperatures for the deconfinement and chiral phase transitions coincide. On the contrary, for gauge theories with adjoint matter the two transition temperatures can be very different [9,10].

To clarify the relevance of the center for confinement it suggests itself to study pure gauge theories whose gauge groups have a trivial center. For such theories the string connecting external charges can break via the spontaneous creation of dynamical ''gluons'' such that the Polyakov loop acquires a nonvanishing expectation value for all

*Bjoern.Wellegehausen@uni-jena.de
†A.Wipf@tpi.uni-jena.de
‡Christian.Wozar@uni-jena.de

TABLE I. Centers $\mathcal{Z}$ of simple lie groups.

Group	A_r	B_r	C_r	D_r, r even	D_r, r odd	E_6	E_7	E_8	F_4	G_2
Center $\mathcal{Z}$	$\mathbb{Z}_{r+1}$	$\mathbb{Z}_2$	$\mathbb{Z}_2$	$\mathbb{Z}_2 \times \mathbb{Z}_2$	$\mathbb{Z}_4$	$\mathbb{Z}_3$	$\mathbb{Z}_2$	$\mathbb{1}$	$\mathbb{1}$	$\mathbb{1}$

temperatures, similarly as it does in QCD with dynamical fermions. Here the simple gauge group $SO(3)$ suggests itself and indeed the $SO(3)$ gauge theory has been studied in great detail on the lattice, see, for example, [11]. Unfortunately, via the nontrivial first homotopy group $\pi_1(SO(3)) = \mathbb{Z}_2$ the lattice gauge theory "detects" its simply connected universal covering group $SU(2)$. To avoid the resulting lattice artifacts one should investigate theories with simply connected gauge groups with a trivial center.

From Table I, taken from [12], one reads off that the smallest simple Lie group with these properties is the 14 dimensional exceptional Lie group G_2. This is one reason why the group in Bern investigated G_2 gauge theories with and without Higgs fields in a series of papers [13–15]. In their pioneering works it has been convincingly demonstrated that G_2 gluodynamics shows a first order finite temperature phase transition without an order parameter from a confining to a deconfining phase. In this context confinement refers to confinement at intermediate scales, where a Casimir scaling of string tensions has been reported [16]. On large scales strings will finally break due to spontaneous gluon production and the static interquark potential is expected to flatten [17]. However, the threshold energy for string breaking in G_2 gauge theory is rather high and all previous attempts to detect this flattening have been without success. In the present paper we shall demonstrate that string breaking for charges in the fundamental and adjoint representations of G_2 takes place at the expected scales. To that aim we implemented a slightly modified Lüscher-Weisz multistep algorithm for high precision measurements of the static interquark potential.

The present paper deals with G_2 gluodynamics in 3 and 4 dimensions. The simulations are performed with an efficient and fast implementation of a local hybrid Monte Carlo algorithm. Below we shall calculate the potentials at intermediate scales for static charges in the 7, 14, 27, 64, 77, 77′, 182, and 189 dimensional representations. We show that in 3 and 4 dimensions the string tensions on intermediate scales are proportional to the second order Casimir of the representations. The high precision measurements in 3 dimensions confirm Casimir scaling within 4% for all mentioned representations. In 4 dimensions Casimir scaling for the lowest 4 representations is again fulfilled within 5%. In 3 dimensions we also calculated the static potential for widely separated charges in the two fundamental representations. In both cases we see a flattening of the potential which signals the breaking of the connecting string. The energy where string breaking sets in is in full agreement with the independently calculated masses of the glue lumps formed after string breaking. Interestingly, in the region close to the string breaking distance Casimir scaling for the fundamental charges is found to be violated by about 2.5%. Eventually the continuum extrapolated numerical value of the string tension in 3 dimensions is found to be in good agreement with analytical predictions.

II. THE GROUP G_2

The exceptional Lie group G_2 is the automorphism group of the octonion algebra or, equivalently, the subgroup of $SO(7)$ that preserves any vector in its 8 dimensional real spinor representation. This means that the 8 dimensional real spinor representation of Spin(7) branches into the trivial representation and the 7 dimensional fundamental representation of G_2. The 14 dimensional fundamental representation of G_2, which at the same time is the adjoint representation, arises in the branching of the adjoint of $SO(7)$ according to $21 \to 7 \oplus 14$. The 27 dimensional representations of $SO(7)$ acting on symmetric traceless 2-tensors remains irreducible under G_2. In this work we need the following *branchings* of $SO(7)$ representations to G_2:

$$7 \to 7, \qquad 21 \to 14 \oplus 7, \qquad 27 \to 27,$$
$$35 \to 27 \oplus 7 \oplus 1, \qquad 77 \to 77. \tag{2}$$

For explicit calculations it is advantageous to view the elements of the 7 dimensional representation of G_2 as matrices in the defining representation of $SO(7)$, subject to seven independent cubic constraints [15]

$$T_{abc} = T_{def} g_{da} g_{eb} g_{fc}. \tag{3}$$

Here T is a total antisymmetric tensor given by

$$T_{127} = T_{154} = T_{163} = T_{235} = T_{264} = T_{374} = T_{576} = 1. \tag{4}$$

The gauge group $SU(3)$ of strong interaction is a subgroup of G_2 and the corresponding coset space is a sphere [18],

$$G_2/SU(3) \sim S^6. \tag{5}$$

This means that every element $\mathcal{U}$ of G_2 can be factorized as

$$\mathcal{U} = \mathcal{S} \cdot \mathcal{V} \text{ with } \mathcal{V} \in SU(3) \text{ and } \mathcal{S} \in G_2/SU(3), \tag{6}$$

and we shall use this decomposition in our simulations. The short exact sequence

$$0 = \pi_4(S^6) \to \pi_3(SU(3)) \to \pi_3(G_2) \to \pi_3(S^6) = 0 \tag{7}$$

shows that $\pi_3(G_2) = \mathbb{Z}$ and hence there should exist G_2 instantons of any integer topological charge. In the

TABLE II. Representations of G_2 with corresponding dimension and Casimir values.

Representation $\mathcal{R}$	[1,0]	[0,1]	[2,0]	[1,1]	[3,0]	[0,2]	[4,0]	[2,1]
Dimension $d_{\mathcal{R}}$	7	14	27	64	77	77′	182	189
Casimir eigenvalue $\mathcal{C}_{\mathcal{R}}$	12	24	28	42	48	60	72	64
Casimir ratio $\mathcal{C}'_{\mathcal{R}}$	1	2	7/3	3.5	4	5	6	16/3

charge k sector there are at least $3k$ magnetically charged defects [12].

Any irreducible representation of G_2 is characterized by its highest weight vector μ which is a linear combination of the fundamental weights, $\mu = p\mu_{(1)} + q\mu_{(2)}$, with non-negative integer coefficients p, q called Dynkin labels. The dimension of an arbitrary irreducible representation $\mathcal{R} = [p, q]$ can be calculated with the help of Weyl's dimension formula and is given by

$$\begin{aligned} d_{\mathcal{R}} &\equiv \dim_{p,q} \\ &= \frac{1}{120}(1+p)(1+q)(2+p+q)(3+p+2q) \\ &\quad \times (4+p+3q)(5+2p+3q). \end{aligned} \tag{8}$$

Below we also use the physics convention and denote a representation by its dimension. For example, the fundamental representations are $[1,0] = 7$ and $[0,1] = 14$. However, this notation is ambiguous, since there exist different representations with the same dimension. For example $[3,0] = 77$ and $[0,2] = 77'$ have the same dimension. An irreducible representation of G_2 can also be characterized by the values of the two Casimir operators of degree 2 and 6. Below we shall need the values of the quadratic Casimir in a representation $[p, q]$, given by

$$\mathcal{C}_{\mathcal{R}} \equiv \mathcal{C}_{p,q} = 2p^2 + 6q^2 + 6pq + 10p + 18q. \tag{9}$$

For an easy comparison we normalize these "raw" Casimir values with respect to the defining representation by $\mathcal{C}'_{p,q} = \mathcal{C}_{p,q}/\mathcal{C}_{1,0}$. The normalized Casimir values for the eight nontrivial representations with smallest dimensions are given in Table II.

Quarks and gluons in G_2 are in the fundamental representations 7 and 14, respectively. To better understand G_2 gluodynamics we recall the decomposition of tensor products of these representations,

$$\begin{aligned} 7 \otimes 7 &= 1 \oplus 7 \oplus 14 \oplus 27, \\ 7 \otimes 14 &= 7 \oplus 27 \oplus 64, \\ 14 \otimes 14 &= 1 \oplus 14 \oplus 27 \oplus 77 \oplus 77', \\ 7 \otimes 7 \otimes 7 &= 1 \oplus 4 \cdot 7 \oplus 2 \cdot 14 \oplus 3 \cdot 27 \oplus 2 \cdot 64 \oplus 77', \\ 14 \otimes 14 \otimes 14 &= 1 \oplus 7 \oplus 5 \cdot 14 \oplus 3 \cdot 27 \oplus \ldots. \end{aligned} \tag{10}$$

The decompositions (10) show that, similarly as in QCD, two or three quarks or two or three gluons can build color singlets—mesons, baryons, or glueballs. Since three gluons can screen the charge of a single (static) quark,

$$7 \otimes 14 \otimes 14 \otimes 14 = 1 \oplus \ldots, \tag{11}$$

one expects that the string between two static quarks will break for large charge separations. The two remnants are two glue lumps—charges screened by (at least) 3 gluons. The same happens for charges in the adjoint representation. Each adjoint charge can be screened by one gluon.

Construction of characters from tensor products

The character $\chi_{\mathcal{R}}(\mathcal{U}) = \mathrm{tr}_{\mathcal{R}}(\mathcal{U})$ of any irreducible representation $\mathcal{R}$ is a polynomial of the characters χ_7 and χ_{14} of the two fundamental representations 7 and 14. For example, the first two decompositions in (10) imply

$$\begin{aligned} \chi_{27} &= \chi_7 \cdot \chi_7 - \chi_1 - \chi_7 - \chi_{14}, \\ \chi_{64} &= \chi_7 \cdot \chi_{14} - \chi_7 - \chi_{27} = \chi_7\chi_{14} - \chi_7^2 + \chi_1 + \chi_{14}, \end{aligned} \tag{12}$$

and yield the characters of the representations 27 and 64 as polynomials of χ_7 and χ_{14}. From further tensor products of irreducible representations one can calculate the polynomial in $\chi_{\mathcal{R}} = \mathrm{Pol}_{\mathcal{R}}(\chi_7, \chi_{14})$ for any irreducible representation $\mathcal{R}$. For a fast implementation of our algorithms we also need reducible representations. In particular we use

$$(7 \otimes 7)_s, \quad (7 \otimes 7 \otimes 7)_s, \quad (7 \otimes 7 \otimes 7 \otimes 7)_s, \quad (7 \otimes 7)_s \otimes 14, \tag{13}$$

where the subscript "s" denotes the symmetrized part of the respective tensor product. Comparing the reduction of representations for $SO(7)$ and G_2 and mapping representations from $SO(7)$ to G_2 the following characters of reducible representations can be computed:

$$\begin{aligned} \chi_{(7\otimes 7)_s} &= \chi_{27} + \chi_1, \qquad \chi_{(7\otimes 7\otimes 7)_s} = \chi_{77} + \chi_7, \\ \chi_{(7\otimes 7\otimes 7\otimes 7)_s} &= \chi_{182} + \chi_{77} + \chi_{27} + \chi_{64} + 2\chi_{14} + \chi_7, \\ \chi_{(7\otimes 7)_s\otimes 14} &= \chi_{189} + \chi_{77} + \chi_{27} + \chi_{64} + 2\chi_{14} + \chi_7. \end{aligned} \tag{14}$$

III. CASIMIR SCALING AND STRING BREAKING FOR $SU(N_c)$ GAUGE THEORIES

In QCD quarks and antiquarks can only be screened by particles with nonvanishing 3-ality, especially not by

gluons. Thus, in zero-temperature gluodynamics the potential energy for two static color charges is linearly rising up to arbitrary large separations of the charges. The potentials for charges in a representation $\mathcal{R}$ can be extracted from the 2-point correlator of Polyakov loops or the expectation values of Wilson loops with temporal extent T according to

$$\begin{aligned}\langle P_{\mathcal{R}}(0)P_{\mathcal{R}}(R)\rangle &= \mathrm{e}^{-\beta_T V_{\mathcal{R}}(R)},\\ \langle W_{\mathcal{R}}(R,T)\rangle &= \mathrm{e}^{\kappa_R - TV_{\mathcal{R}}(R)}.\end{aligned} \tag{15}$$

With dynamical quarks the string should break at a characteristic length r_b due to the spontaneous creation of quark antiquark pairs from the energy stored in the flux tube connecting the static charges. However, for intermediate separations $r < r_b$ the string cannot break since there is not enough energy stored in the flux tube.

For pure gauge theories we expect the following qualitative behavior of the static potential: At short distances perturbation theory applies and the interaction is dominated by gluon exchange giving rise to a Coulomb-like potential, $V \sim -\alpha/r$, the strength α being proportional to the value $\mathcal{C}_{\mathcal{R}}$ of the quadratic Casimir operator in the given representation $\mathcal{R}$ of the charges; at intermediate distances, from the onset of confinement to the onset of color screening at r_b, the potential is expected to be linearly rising, $V \sim \sigma r$, and the corresponding string tension is again proportional to the quadratic Casimir; at asymptotic distance scales (partial) screening sets in such that the string tension typically decreases and only depends on the N-ality of the representation. In particular for center-blind color charges or gauge groups without center the potential flattens. The characteristic length r_b where the intermediate confinement regime turns into the asymptotic screening regime is determined by the masses of the debris left after string breaking. The Casimir scaling hypothesis, according to which the string tension at intermediate scales is proportional to the quadratic Casimir of the representation [19], is exact for two dimensional continuum and lattice gauge theories and dimensional reduction arguments support that it also holds in higher dimensions. Within the Hamiltonian approach to Yang-Mills theories in $2+1$ dimensions the following prediction for the string tensions has been derived [20]:

$$\sigma_{\mathcal{R}} = \frac{g^4}{4\pi}\frac{\mathcal{C}_{14}\mathcal{C}_{\mathcal{R}}}{12^2}, \tag{16}$$

with a recent refinement in [21].[1] These analytical results directly predict Casimir scaling in three dimensions. In four dimensions Casimir scaling can be explained via Gaussian field correlators [22]. For pure $SU(2)$ and $SU(3)$ gauge theories in three and four dimensions there is now conclusive numerical evidence for Casimir scaling from Monte Carlo simulations, for $SU(2)$ in 3 dimensions [19,23] and in 4 dimensions [24–27] as well as for $SU(3)$ in 4 dimensions at finite temperature [28] and zero temperature [29–32]. In particular the simulations for $SU(3)$ gluodynamics in [31] confirm Casimir scaling within 5% for separations up to 1 fm of static charges in representations with Casimirs (normalized by the Casimir of {3}) up to 7. String breaking for charges in the adjoint representation has been found in several simulations: In 3 dimensional $SU(2)$ gluodynamics with improved action and different operators in [33,34] and in 4 dimensional $SU(2)$ gluodynamics in [35] with the help of a variational approach involving string and glueball operators. For a critical discussion of the various approaches we refer to [36], where string breaking in a simple setting but with an improved version of the Lüscher-Weisz algorithm has been analyzed and compared with less sophisticated approaches. There is a number of works in which a violation of Casimir scaling on intermediate scales have been reported. For example, it has been claimed that in 4 dimensional $SU(N_c)$ gluodynamics with larger $N_c \in \{4, 6\}$ the numerical data favor the sin formula, as suggested by supersymmetry, in place of the Casimir scaling formula [37]. The differences between the Casimir scaling law and sin-formula are tiny and it is very difficult to discriminate between the two predictions in numerical simulations. Indeed, in [38] agreement with Casimir scaling and the sin formula in 4 dimensions and disagreement in 3 dimensions has been claimed. In addition the high precision simulations based on the Lüscher-Weisz algorithm in [36,39] point to a violation of the Casimir scaling law in 3 dimensional $SU(2)$ gluodynamics. In a very recent paper Pepe and Wiese [40] reanalyzed the static potential for $SU(2)$ gluodynamics in 3 dimensions with the help of the Lüscher-Weisz algorithm and substantiated Casimir scaling violation at intermediate scales while confirming 2-ality scaling at asymptotic scales.

For *gauge theories with matter* we expect a similar qualitative behavior: A Coulomb-like potential at short distances, Casimir scaling at intermediate distances, and (partial) screening at asymptotic distances. The string tension at asymptotic scales depends both on the N-alities of the static color charges and of the dynamical matter. In particular, if dynamical quarks or scalars can form center-blind composites with the static charges then the potential is expected to flatten at large separations. To see any kind of screening between fundamental charges requires a full QCD simulation with sea quarks, which is demanding. Thus, the earlier works dealt with gauge theories with scalars in the fundamental representation. For example, in [41] clear numerical evidence for string breaking in the 3 dimensional $SU(2)$ Yang-Mills–Higgs model via a mixing analysis of string and two-meson operators has been presented. Probably the first observation of hadronic string breaking in simulations of QCD_3 with two flavors of

[1]The factor $1/12^2$ in the formula given here arises from a different normalization of the quadratic Casimir operator.

dynamical staggered fermions using only Wilson loops has been reported in [42,43]. Despite extensive searches for color screening in 4 dimensional gauge theories with dynamical fermions the results are still preliminary at best. First indications for string breaking in two flavor QCD, albeit only at temperatures close to or above the critical deconfinement temperature, have been reported in [44]. More recently Bali *et al.* used sophisticated methods (e.g. optimized smearing, improved action, stochastic estimator techniques, hopping parameter acceleration) to resolve string breaking in two flavor QCD at a value of the lattice spacing $a^{-1} \approx 2.37$ GeV and of the sea quark mass slightly below m_s [45]. By extrapolation they estimate that in real QCD with light quarks the string breaking should happen at $r_b \approx 1.13$ fm.

To measure the static potential and study string breaking three approaches have been used: correlations of Polyakov loops at finite temperature, variational ansaetze using two types of operators (for the stringlike states and for the broken-string state), and Wilson loops. Most results on Casimir scaling and string breaking have been obtained with the first two methods. This is attributed to the small overlap of the Wilson loops with the broken-string state. To measure Polyakov or Wilson loop correlators for charges in higher representations or to see screening at asymptotic scales one is dealing with extremely small signals down to 10^{-40}. In order to measure such small signals one needs to improve existing algorithms considerably or/and use improved versions of the Lüscher-Weisz multistep algorithm.

For *gauge groups with trivial centers* like G_2, F_4, or E_8 the flux tube between static charges in any representation will always break due to gluon production. The potential flattens for large separations and expectation values of the Polyakov loop never vanish [13]. However, for G_2 it changes rapidly at the phase transition temperature and is very small in the low-temperature confining phase, see Fig. 1. Similarly as in QCD we characterize confinement

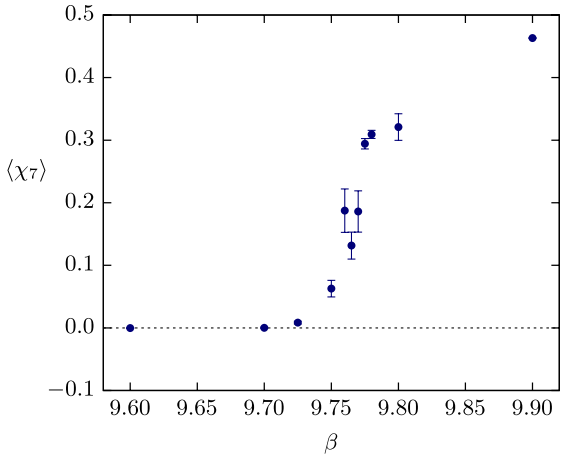

FIG. 1 (color online). Phase transition on a $16^3 \times 6$ lattice in terms of the Polyakov loop in the fundamental representation.

as the absence of free color charges in the physical spectrum [16,46].

IV. ALGORITHMIC CONSIDERATIONS

A. Local hybrid Monte Carlo

In simulations of gauge field theories different algorithms are in use. For $SU(N_c)$ gluodynamics heat-bath algorithms based on the Cabibbo-Marinari $SU(2)$ subgroup updates, often improved by over-relaxation steps, have proven to be fast and reliable. For QCD with dynamical fermions a hybrid Monte Carlo (HMC) scheme is preferable. Based on [47] also local versions of HMC algorithms are available where single links are evolved in a HMC style. According to [48] the cost for the local hybrid Monte Carlo (LHMC) is about 3 times more than for a combined heat-bath and over-relaxation scheme for the case of $SU(N_c)$ gluodynamics.

For the exceptional gauge group G_2 there exists a modification of the heat-bath update [13] which combines the heat-bath update for a $SU(3)$ subgroup with randomly distributed G_2 gauge transformations to rotate the $SU(3)$ subgroup through G_2. In the present work we instead use a LHMC algorithm for several good reasons: First, the formulation is given entirely in terms of the Lie group and Lie algebra elements and there is no need to back-project onto G_2. The autocorrelation time can be controlled (in certain ranges) by the integration time in the molecular dynamics part of the HMC algorithm. Furthermore, one can use a real representation of G_2 and relatively simple analytical expressions for the two involved exponential maps to obtain a fast implementation of the algorithm. Finally, the inclusion of a (normalized) Higgs field is straightforward and does not suffer from a low Metropolis acceptance rate (even for large hopping parameters).

The LHMC algorithm has been essential for obtaining the results in the present work. Since we developed the first implementation for G_2 it is useful to explain the technical details for this exceptional group. As any (L)HMC algorithm for gauge theories it is based on a fictitious dynamics for the link-variables on the gauge group manifold. The "free evolution" on a semisimple group is the Riemannian geodesic motion with respect to the Cartan-Killing metric

$$ds_G^2 = \kappa \,\mathrm{tr}(d\mathcal{U}\mathcal{U}^{-1} \otimes d\mathcal{U}\mathcal{U}^{-1}). \tag{17}$$

In the fictitious dynamics the interaction term is given by the Yang-Mills action of the underlying lattice gauge theory and hence it suggests itself to derive the dynamics from the Lagrangian

$$L = \frac{1}{2}\sum_{x,\mu} \mathrm{tr}(i\dot{\mathcal{U}}_{x,\mu}\mathcal{U}_{x,\mu}^{-1})^2 - S_{\mathrm{YM}}[\mathcal{U}], \tag{18}$$

where "dot" denotes the derivative with respect to the fictitious time parameter τ and

$$S_{\mathrm{YM}}[\mathcal{U}] = \frac{\beta}{2N_c}\sum_{x,\mu\nu}\mathrm{tr}(2N_c - \mathcal{U}_{x,\mu\nu} - \mathcal{U}^{\dagger}_{x,\mu\nu}),$$
$$\beta = \frac{2N_c}{ag^2}, \tag{19}$$

is the Wilson action. The Lie algebra valued fictitious *conjugated link momentum* is given by

$$\mathfrak{P}_{x,\mu} = i\frac{\partial L}{\partial(\dot{\mathcal{U}}_{x,\mu}\mathcal{U}^{-1}_{x,\mu})} = i\mathcal{U}_{x,\mu}\frac{\partial L}{\partial\dot{\mathcal{U}}_{x,\mu}} = -i\dot{\mathcal{U}}_{x,\mu}\mathcal{U}^{-1}_{x,\mu}, \tag{20}$$

and via a Legendre transform yields the pseudo-Hamiltonian

$$H = \frac{1}{2}\sum_{x,\mu}\mathrm{tr}\,\mathfrak{P}^2_{x,\mu} + S_{\mathrm{YM}}[\mathcal{U}]. \tag{21}$$

The equations of motion for the momenta are obtained by varying the Hamiltonian. The variation of the Wilson action $S_{\mathrm{YM}}[\mathcal{U}]$ with respect to a fixed link variable $\mathcal{U}_{x,\mu}$ is given by the corresponding staple variable $R_{x,\mu}$, the sum of triple products of elementary link variables closing to a plaquette with the chosen link variable. Hence we obtain

$$\delta H = \sum_{x,\mu}\mathrm{tr}\{\mathfrak{P}_{x,\mu}\delta\mathfrak{P}_{x,\mu} + i\delta\mathcal{U}_{x,\mu}\mathcal{U}^{\dagger}_{x,\mu}F_{x,\mu}\}$$
$$= \sum_{x,\mu}\mathrm{tr}\,\mathfrak{P}_{x,\mu}\{\dot{\mathfrak{P}}_{x,\mu} - F_{x,\mu}\}d\tau,$$
$$F_{x,\mu} = \frac{i\beta}{2N_c}(\mathcal{U}_{x,\mu}R_{x,\mu} - R^{\dagger}_{x,\mu}\mathcal{U}^{\dagger}_{x,\mu}). \tag{22}$$

The variational principle implies that the projection of the term between curly brackets onto the Lie algebra $\mathfrak{g}_2$ vanishes,

$$\dot{\mathfrak{P}}_{x,\mu} = F_{\mu,x}|_{\mathfrak{g}_2}. \tag{23}$$

Choosing a trace-orthonormal basis $\{T_a\}$ of $\mathfrak{g}_2$ the equations for the (L)HMC dynamics can be written as follows:

$$\dot{\mathfrak{P}}_{x,\mu} = \sum_a \mathrm{tr}(F_{x,\mu}T_a)T_a \quad \text{and} \quad \dot{\mathcal{U}}_{x,\mu} = i\mathfrak{P}_{x,\mu}\mathcal{U}_{x,\mu}, \tag{24}$$

with the "force" $F_{x,\mu}$ defined in (22). Now a LHMC sweep consists of the following steps:

(1) Gaussian draw of the momentum variable on a given link,
(2) Integration of the equations of motion for the given link,
(3) Metropolis accept/reject step,
(4) Repeat these steps for all links of the lattice.

This local version of the HMC does not suffer from an extensive $\delta H \propto V$ problem such that already a second order symplectic (leap frog) integrator allows for sufficiently large timesteps $\delta\tau$. In its condensed form the integration for a link variable yields

$$\mathcal{U}(t+\delta\tau) = \exp(i\mathfrak{P}(t+\delta\tau/2)\delta\tau)\mathcal{U}(t). \tag{25}$$

For a large range of Wilson couplings β in our simulations an integration length of $T = 0.75$ with a step size of $\delta\tau = 0.25$ is optimal for minimal autocorrelation times and a small number of thermalization sweeps. Acceptance rates of more than 99% are reached. Nevertheless, the most time consuming part of the calculations involves the exponential maps. A calculation for G_2 can be implemented fast and exact up to a given order in $\delta\tau$ as will be shown in the next section.

B. The exponential map $\mathfrak{g}_2 \to G_2$

For an efficient and fast computation of the exponential map we use the *real embedding* of the $SU(3)$ representation $3 \oplus \bar{3}$ into G_2, given by

$$\mathcal{V}(\mathcal{W}) = \Omega^{\dagger}\begin{pmatrix}1 & 0 & 0\\ 0 & \mathcal{W} & 0\\ 0 & 0 & \mathcal{W}^*\end{pmatrix}\Omega \in G_2 \ \text{ with } \ \mathcal{W} \in SU(3). \tag{26}$$

One can choose the unitary matrix Ω to have block diagonal form with $\Omega_{11} = 1$. A possible choice for Ω is

$$\Omega = \begin{pmatrix}1 & 0\\ 0 & VQ\end{pmatrix} \quad \text{with} \quad Q = \begin{pmatrix}0&0&0&0&0&1\\0&0&1&0&0&0\\1&0&0&0&0&0\\0&0&0&0&1&0\\0&0&0&1&0&0\\0&1&0&0&0&0\end{pmatrix},$$
$$V = \frac{1}{\sqrt{2}}\begin{pmatrix}1 & i\\ i & 1\end{pmatrix}\otimes\mathbb{1}_3. \tag{27}$$

Every element of G_2 can be factorized as

$$\mathcal{U} = \mathcal{S}\cdot\mathcal{V}(\mathcal{W}) \quad \text{with} \quad \mathcal{S} \in G_2/SU(3). \tag{28}$$

For a given timestep $\delta\tau$ in the molecular dynamics this factorization will be expressed in terms of the Lie algebra elements with the help of the exponential maps,

$$\exp\{\delta\tau\mathfrak{u}\} = \exp\{\delta\tau\mathfrak{s}\}\cdot\exp\{\delta\tau\mathfrak{v}\}$$
$$\text{with generators } \mathfrak{u} \in \mathfrak{g}_2, \qquad \mathfrak{v} \in \mathcal{V}_*(\mathfrak{su}(3)) \tag{29}$$

fulfilling the commutation relations

$$[\mathfrak{v},\mathfrak{v}'] = \mathfrak{v}'', \quad [\mathfrak{v},\mathfrak{s}] = \mathfrak{s}', \ \text{ and } \ [\mathfrak{s},\mathfrak{s}'] = \mathfrak{v}' + \mathfrak{s}''. \tag{30}$$

The generators $\mathfrak{s}$ are orthogonal to the generators of the really embedded $SU(3)$ subgroup. To simplify the notation we absorb the time step $\delta\tau$ in the Lie algebra elements.

The last exponential map in (29) can be calculated with the help of the embedding (26) and the exponential map for $SU(3)$, $\mathcal{W} = \exp(\mathfrak{w})$, which follows from the Cayley-Hamilton theorem for $SU(3)$ generators, see [49]. The result can be expressed in terms of the imaginary eigenvalues w_1, w_2, w_3 of $\mathfrak{w}$ and the differences $\delta_1 = w_2 - w_3$, $\delta_2 = w_3 - w_1$, and $\delta_3 = w_1 - w_2$ by

$$\mathcal{W} = \exp(\mathfrak{w}) = -\frac{1}{\delta_1\delta_2\delta_3}(\alpha_{\mathbb{1}}\mathbb{1} + \alpha_{\mathfrak{w}}\mathfrak{w} + \alpha_{\mathfrak{w}^2}\mathfrak{w}^2), \tag{31}$$

with expansion coefficients

$$\alpha 1 = \sum_{i=1}^{3} \delta_i w_{i+1} w_{i+2} e^{w_i}, \qquad \alpha_{\mathfrak{w}} = \sum_{i=1}^{3} \delta_i w_i e^{w_i},$$
$$\alpha_{\mathfrak{w}^2} = \sum_{i=1}^{3} \delta_i e^{w_i}, \tag{32}$$

wherein one identifies w_{3+i} and w_i.

For the generators $\{\mathfrak{u}_1, \ldots, \mathfrak{u}_{14}\}$ of G_2 we use the real representation given in [46]. The $\mathfrak{su}(3)$ subalgebra formed by the elements $\{\mathfrak{u}_1, \ldots, \mathfrak{u}_8\}$ generates the really embedded $3 \oplus \bar{3}$ of $SU(3)$ and the remaining generators $\{\mathfrak{u}_9, \ldots, \mathfrak{u}_{14}\}$ generate the coset elements $\mathcal{S}$ in the factorization (28). With this choice for the generators the real embedding (26) reads

$$\mathcal{V}(\mathcal{W}) = \begin{pmatrix} 1 & 0 \\ 0 & \mathcal{V}_\perp \end{pmatrix},$$
$$\mathcal{V}_\perp = \begin{pmatrix} a_{33} & -b_{33} & a_{32} & -b_{32} & -b_{31} & a_{31} \\ b_{33} & a_{33} & b_{32} & a_{32} & a_{31} & b_{31} \\ a_{23} & -b_{23} & a_{22} & -b_{22} & -b_{21} & a_{21} \\ b_{23} & a_{23} & b_{22} & a_{22} & a_{21} & b_{21} \\ b_{13} & a_{13} & b_{12} & a_{12} & a_{11} & b_{11} \\ a_{13} & -b_{13} & a_{12} & -b_{12} & -b_{11} & a_{11} \end{pmatrix}, \tag{33}$$

where the entries are the real and imaginary parts of the elements of the $SU(3)$ matrix, $\mathcal{W}_{ij} = a_{ij} + ib_{ij}$.

Finally, to parametrize the elements of the coset space we calculate the remaining exponential map

$$\mathcal{S} = \exp\{\mathfrak{s}\} \quad \text{with} \quad \mathfrak{s} = \sum_{i=1}^{i=6} s_i \mathfrak{u}_{8+i}. \tag{34}$$

The result depends on the real parameter $\sigma = \| \vec{s} \|$ and the 6 dimensional unit vector $\hat{s} = \vec{s}/\| \vec{s} \|$. In a 1×6-block notation the map takes the form

$$\mathcal{S} = \begin{pmatrix} \cos 2\sigma & -\sin 2\sigma \hat{s}T \\ \sin 2\sigma \hat{s} & \mathcal{S}_\perp \end{pmatrix}, \tag{35}$$

with a 6 dimensional matrix

$$S_\perp = \cos\sigma \mathbb{1} + \sin\sigma \hat{\mathfrak{s}}_\perp + (\cos 2\sigma - \cos\sigma)\hat{s}\hat{s}^{\mathsf{T}} + (1 - \cos\sigma)\hat{v}\hat{v}^{\mathsf{T}}. \tag{36}$$

The matrix $\hat{\mathfrak{s}}_\perp$ is the 6×6 right-lower block of $\mathfrak{s}$ in (34). The unit vector $\hat{v}^{\mathsf{T}} = (\hat{s}_2, -\hat{s}_1, \hat{s}_4, -\hat{s}_3, -\hat{s}_6, \hat{s}_5)$ defining the last projector in (36) is orthogonal to the unit vector $\hat{s}$ defining the projector $\hat{s}^{\mathsf{T}}$.

In the numerical integration we need the exponential map for elements $\mathfrak{u}$ in $\mathfrak{g}_2$. They are related to the generators used in the factorization by the Baker-Campbell-Hausdoff formula,

$$\delta\tau\mathfrak{u} = \delta\tau(\mathfrak{s} + \mathfrak{v}) + \tfrac{1}{2}\delta\tau^2[\mathfrak{s}, \mathfrak{v}] + \ldots. \tag{37}$$

Depending on the order of the symplectic integrator we must solve this relation for $\mathfrak{s}$ and $\mathfrak{v}$ up to the corresponding order in $\delta\tau$. For a second order integrator used in this work this can be done analytically since the commutator $[\mathfrak{s}, \mathfrak{v}]$ does not contain any contribution of the subalgebra $\mathfrak{su}(3)$. The integrator used in the (L)HMC algorithm must be time reversible. It can be checked that time reversibility holds to every order in this expansion. To summarize, for a second order integrator the approximation (37) may be used in the exponentiations needed to calculate $\mathcal{V}$ and $\mathcal{S}$. This approximation leads to a violation of energy conservation, which is of the same order as the violation one finds with a second order integrator. In comparison to the exponentiation via the spectral decomposition the method based on the factorization (28) is more than 10 times faster. It is also much faster than computing the exponential map for $SO(7)$ via the Cayley-Hamilton theorem.

C. Exponential error reduction for Wilson loops

In the confining phase the rectangular Wilson loop scales as $W(L, T) \propto \exp(-\sigma L \cdot T)$. In order to estimate the string tension σ we probe areas LT ranging from 0 up to 100 and thus W will vary by approximately 40 orders of magnitude. A brute force approach where statistical errors for the expectation value of Wilson or Polyakov loops decrease with the inverse square root of the number of statistically independent configurations by just increasing the number of generated configurations will miserably fail. Nevertheless, convincing results on G_2 Casimir scaling on intermediate scales for representations with relative Casimirs $C'_{\mathcal{R}} \leq 5$ have been obtained in [16] with a variant of the smearing procedure. When reproducing these results we observed that the calculated string tensions depend sensitively on the smearing parameter.[2] Thus, to obtain accurate and reliable numbers for the static potential and to detect string breaking we implemented the multistep Lüscher-Weisz algorithm with exponential error reduction for the time transporters of the Wilson loops [50]. With this method the absolute errors of Wilson lines decrease

[2]This is not the case for the ratios of string tensions.

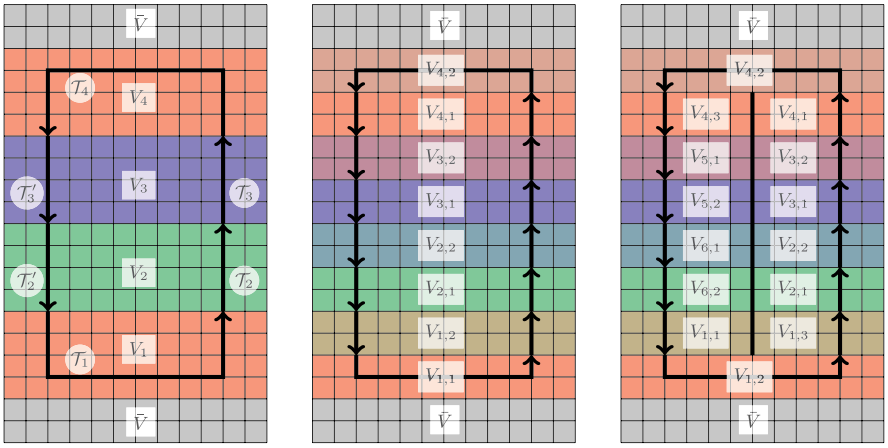

FIG. 2 (color online). Iterative slicing (from left to right) of a lattice and Wilson loop during the multilevel algorithm.

exponentially with the temporal extent T of the line. This is achieved by subdividing the lattice into n_t sublattices $V_1, \ldots, V_{n_t}$ containing the Wilson loop and separated by time slices plus the remaining sublattice, denoted by $\bar{V}$, see Fig. 2 (left panel). At the first level in a two-level algorithm the time extent of each sublattice V_n is 4 such that n_t is the smallest natural number with $4n_t \geq T + 2$. In Fig. 2 (left panel) $T = 14$ and the lattice is split into four sublattices V_1, V_2, V_3, V_4 containing the Wilson loop plus the complement $\bar{V}$. The Wilson loop is the product of parallel transporters $W = \mathcal{T}_2'\mathcal{T}_3'\mathcal{T}_4\mathcal{T}_3\mathcal{T}_2\mathcal{T}_1$. If a sublattice V_n contains only one connected piece of the Wilson loop (as V_1 and V_4 do) then one needs to calculate the sublattice expectation value

$$\langle \mathcal{T}_n \rangle_n = \frac{1}{Z_n} \int_{\text{sublattice } n} \mathcal{D}\mathcal{U}\mathcal{T}_n e^{-S}, \tag{38}$$

if V_n contains two connected pieces (as V_2 and V_3) then one needs to calculate $\langle \mathcal{T}_n \otimes \mathcal{T}_n' \rangle_n$. The updates in each sublattice are done with fixed link variables on the time slices bounding the sublattice. Calculating the expectation value of the full Wilson loop reduces to averaging over the links in the $n_t + 1$ time slices,

$$\langle W \rangle = \langle \mathcal{C}(\langle \mathcal{T}_1 \rangle_1 \langle \mathcal{T}_2 \otimes \mathcal{T}_2' \rangle_2 \cdots \langle \mathcal{T}_{n_t-1} \otimes \mathcal{T}_{n_t-1}' \rangle_{n_t-1} \times \langle \mathcal{T}_{n_t} \rangle_{n_t}) \rangle_{\text{boundaries}}. \tag{39}$$

Here $\mathcal{C}$ is that particular contraction of indices that leads to the trace of the product $W = \mathcal{T}_2' \ldots \mathcal{T}_{n_t-1}' \times \mathcal{T}_{n_t}\mathcal{T}_{n_t-1} \ldots \mathcal{T}_2\mathcal{T}_1$. In a two-level algorithm each sublattice V_n is further divided into two sublattices $V_{n,1}$ and $V_{n,2}$, see Fig. 2 (middle panel), and the sublattice updates are done on the small sublattices $V_{n,k}$ with fixed link variables on the time slices separating the sublattices $V_{n,k}$. This way one finds two levels of nested averages. Iterating this procedure gives the *multilevel algorithm*. Since the dimensions $d_{\mathcal{R}}$ grow rapidly with the Dynkin labels $[p, q]$—for example, below we shall verify Casimir scaling for charges in the 189 dimensional representation [2,1]—it is difficult to store the many expectation values of tensor products of parallel transporters. Thus we implemented a slight modification of the Lüscher-Weisz algorithm where the lattice is further split by spatially slicing along a hyperplane orthogonal to the plane defined by the Wilson loop, see Fig. 2 (right panel). The sublattice updates are done with fixed link variables on the same time slices as before and in addition to the newly introduced space slice. Instead of n_t sublattices containing the Wilson loop we now have $2n_t - 2$ sublattices. But now every sublattice contains only one connected part of the Wilson loop and (39) is replaced by

$$\langle W \rangle = \left\langle \text{tr} \prod_{n=1}^{2n_t-2} \langle \mathcal{T}_n \rangle_n \right\rangle_{\text{boundaries}}. \tag{40}$$

An iteration of this procedure by additional splittings of the time slices leads again to a multilevel algorithm. In the present work we use a two-level algorithm with time slices of length 4 on the first and length 2 on the second level. We calculate $\langle W \rangle$ for Wilson loops (and hence transporters $\mathcal{T}_n$) of varying sizes and in different representations. To avoid the storage of tensor products of large representations we implemented the modified algorithm as explained above.

We also applied the Lüscher-Weisz algorithm to calculate the correlators of two Polyakov loops $\langle P_{\mathcal{R}}(0) P_{\mathcal{R}}(R) \rangle$ on larger lattices. In this case the complete lattice is divided into sublattices separated by time slices, hence there is no complement $\bar{V}$. Since the Polyakov loops are only used for lower-dimensional representations we have not split the lattice by a spatial slicing but used tensor products similar to Eq. (54). Actually for the calculations of Polyakov loop correlators we used the three step Lüscher-Weisz algorithm.

V. STRING TENSION AND CASIMIR SCALING IN G_2 GLUODYNAMICS

The static interquark potential is linearly rising on intermediate distances and the corresponding string tension will depend on the representation of the static charges. We expect to find Casimir scaling where the string tensions for different representations $\mathcal{R}$ and $\mathcal{R}'$ scale according to

$$\frac{\sigma_{\mathcal{R}}}{c_{\mathcal{R}}} = \frac{\sigma_{\mathcal{R}'}}{c_{\mathcal{R}'}} \tag{41}$$

with quadratic Casimir $c_{\mathcal{R}}$. Although all string tensions will vanish at asymptotic scales it is still possible to check for Casimir scaling at intermediate scales where the linearity of the interquark potential is nearly fulfilled.

To extract the static quark antiquark potential two different methods are available. The first makes use of the behavior of rectangular Wilson loops in representation $\mathcal{R}$ for large T,

$$\begin{aligned} &\langle W_{\mathcal{R}}(R,T)\rangle = \exp(\kappa_{\mathcal{R}}(R) - V_{\mathcal{R}}(R)T) \\ &\text{with } V_{\mathcal{R}}(R) = \gamma_{\mathcal{R}} - \frac{\alpha_{\mathcal{R}}}{R} + \sigma_{\mathcal{R}}R. \end{aligned} \tag{42}$$

The potential can be extracted from the ratio of two Wilson loops with different time extent according to

$$V_{\mathcal{R}}(R) = \frac{1}{\tau}\ln\frac{\langle W_{\mathcal{R}}(R,T)\rangle}{\langle W_{\mathcal{R}}(R,T+\tau)\rangle}. \tag{43}$$

We calculated the expectation values of Wilson loops with the two-level Lüscher-Weisz algorithm and fitted the right-hand side of (43) with the potential $V_{\mathcal{R}}(R)$ in (42). The fitting has been done for external charges separated by one lattice unit up to separations R with acceptable signal to noise ratios. From the fits we extracted the constants $\gamma_{\mathcal{R}}$, $\alpha_{\mathcal{R}}$, and $\sigma_{\mathcal{R}}$ entering the static potential. For an easier comparison of the numerical results on lattices of different size and for different values of β we subtracted the constant contribution to the potentials and plotted

$$\tilde{V}_{\mathcal{R}}(R) = V_{\mathcal{R}}(R) - \gamma_{\mathcal{R}} \tag{44}$$

in the figures. The statistical errors are determined with the Jackknife method. In addition we determined the *local string tension*

$$\sigma_{\mathrm{loc},\mathcal{R}}\left(R+\frac{\rho}{2}\right) = \frac{V_{\mathcal{R}}(R+\rho) - V_{\mathcal{R}}(R)}{\rho}, \tag{45}$$

given by the Creutz ratio

$$\begin{aligned} \sigma_{\mathrm{loc},\mathcal{R}}\left(R+\frac{\rho}{2}\right) &= \frac{\alpha_{\mathcal{R}}}{R(R+\rho)} + \sigma_{\mathcal{R}} \\ &= \frac{1}{\tau\rho}\ln\frac{\langle W_{\mathcal{R}}(R+\rho,T)\rangle\langle W_{\mathcal{R}}(R,T+\tau)\rangle}{\langle W_{\mathcal{R}}(R+\rho,T+\tau)\rangle\langle W_{\mathcal{R}}(R,T)\rangle}. \end{aligned} \tag{46}$$

The second method to calculate the string tensions uses correlators of two Polyakov loops,

$$V_{\mathcal{R}}(R) = -\frac{1}{\beta_T}\ln\langle P_{\mathcal{R}}(0)P_{\mathcal{R}}(R)\rangle. \tag{47}$$

The correlators are calculated with the three-level Lüscher-Weisz algorithm and are fitted with the static potential $V_{\mathcal{R}}(R)$ with fit parameters $\gamma_{\mathcal{R}}$, $\alpha_{\mathcal{R}}$, and $\sigma_{\mathcal{R}}$. Now the local string tension takes the form

$$\sigma_{\mathrm{loc},\mathcal{R}}\left(R+\frac{\rho}{2}\right) = -\frac{1}{\beta_T\rho}\ln\frac{\langle P_{\mathcal{R}}(0)P_{\mathcal{R}}(R+\rho)\rangle}{\langle P_{\mathcal{R}}(0)P_{\mathcal{R}}(R)\rangle}. \tag{48}$$

A. Casimir scaling in 3 dimensions

Most LHMC simulations are performed on a 28^3 lattice with Wilson loops of time extent $T = 12$. To extract the static potentials from the ratio of Wilson loops in (43) we chose $\tau = 2$. The fits to the static potential (42) for charges in the *fundamental 7 representation* and for values $\beta = 30$, 35, and 40 yield the lattice parameters α, γ, and σ given in Table III. To check for scaling we plotted the potentials in "physical" units, V/μ, with mass scale set by the string tension in the 7 representation,

$$\mu = \sqrt{\sigma_7}, \tag{49}$$

as function of μR in Fig. 3. We observe that the potentials for the three values of β are the same within error bars. In addition they agree with the potential (in physical units) extracted from the Polyakov loop on a much larger 48^3 lattice.

The fitted constants $\alpha_{\mathcal{R}}$, $\gamma_{\mathcal{R}}$, and $\sigma_{\mathcal{R}}$ of the potential (42) for the eight smallest representations are given in Table IV. The Casimir scaling of coefficients becomes apparent when they are divided by the corresponding coefficients of the static potential in the 7 representation.

The local string tensions extracted from the Creutz ratio can be determined much more accurately as the global string tensions extracted from fits to the static potentials. Table V contains the local string tensions for static charges in the eight smallest representations for $\rho = 1$ and different R in (46), divided by the corresponding local string

TABLE III. Potential for charges in the 7 representation.

	$\beta = 30$, $N = 28^3$	$\beta = 35$, $N = 28^3$	$\beta = 40$, $N = 28^3$	$\beta = 30$, $N = 48^3$	$\beta = 40$, $N = 64^3$	$\beta = 20$, $N = 32^3$
γa	0.185(8)	0.160(4)	0.147(5)	0.197(1)	0.164(1)	0.252(1)
α	0.0881(1)	0.0752(3)	0.071(4)	0.098(1)	0.0887(1)	0.117(1)
σa^2	0.046(1)	0.0340(8)	0.024(1)	0.0435(3)	0.0221(3)	0.1161(2)

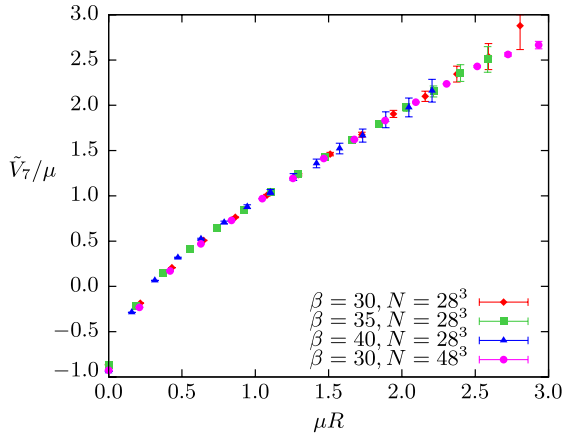

FIG. 3 (color online). Continuum scaling of the fundamental potential.

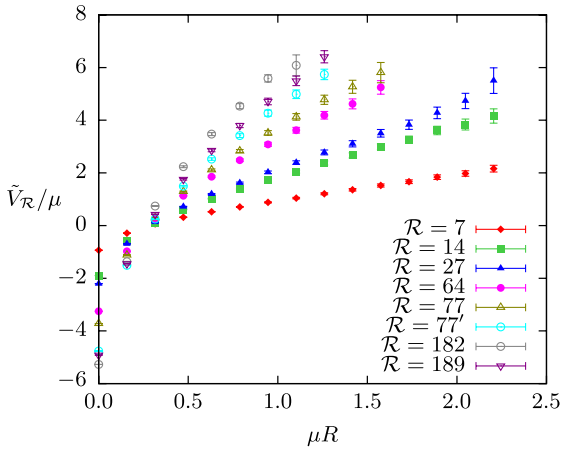

FIG. 4 (color online). Unscaled potential with $\beta = 40$ on a 28^3 lattice.

tensions in the 7 representation. The results are insensitive to the distance R in the Creutz ratio. They agree within 1% with the values for the Casimir ratios $\mathcal{C}'_\mathcal{R} = \mathcal{C}_\mathcal{R}/\mathcal{C}_7$ given in the last row of that table.

In Fig. 4 we plotted the values for the eight potentials $V_7, \ldots, V_{189}$ (with statistical errors) measured in "physical units" μ defined in (49). The distance of the charges is measured in the same system of units. The linear rise at intermediate scales is clearly visible, even for charges in the 189 dimensional representation.

Figure 5 contains the same data points rescaled with the quadratic Casimirs of the corresponding representations. The eight rescaled potentials fall on top of each other within error bars. This implies that the *full potentials* for short and intermediate separations of the static charges show Casimir scaling.

To further check for Casimir scaling we calculated the local string tensions with $\rho = 1$, this time for all R between 1 and 10 and not only for $R = 0$, 1, 2 as in Table V. The horizontal lines in Fig. 6 are the values predicted by the Casimir scaling hypothesis. Clearly we see no sign of Casimir scaling violation on a 28^3 lattice near the continuum at $\beta = 40$. Of course, for widely separated charges in higher-dimensional representations the error bars are not negligible even for an algorithm with exponential error reduction.

TABLE IV. Fit parameters of static potentials.

$\mathcal{R}$	7	14	27	64	77	$77'$	182	189
$\gamma_\mathcal{R} a$	0.147(5)	0.29(1)	0.34(1)	0.51(1)	0.58(1)	0.74(2)	0.83(1)	0.77(2)
$\gamma_\mathcal{R} a/\mathcal{C}'_\mathcal{R}$	0.147	0.145	0.146	0.146	0.145	0.148	0.138	0.144
$\gamma_\mathcal{R}/\gamma_7$	1	1.97	2.31	3.46	3.94	5.03	5.64	5.23
$\alpha_\mathcal{R}$	0.071(4)	0.145(8)	0.16(1)	0.24(1)	0.27(1)	0.36(1)	0.37(1)	0.36(1)
$\alpha_\mathcal{R}/\mathcal{C}'_\mathcal{R}$	0.071	0.0725	0.069	0.069	0.068	0.072	0.062	0.068
$\alpha_\mathcal{R}/\alpha_7$	1	2.04	2.25	3.38	3.80	5.07	5.21	5.07
$\sigma_\mathcal{R} a^2$	0.024(1)	0.048(2)	0.057(3)	0.086(4)	0.099(5)	0.120(6)	0.157(6)	0.132(6)
$\sigma_\mathcal{R} a^2/\mathcal{C}'_\mathcal{R}$	0.024	0.024	0.024	0.025	0.025	0.024	0.026	0.025
$\sigma_\mathcal{R}/\sigma_7$	1	2.00	2.37	3.58	4.12	5.00	6.54	5.50

TABLE V. Scaled local string tension.

$\mathcal{R}$	7	14	27	64	77	$77'$	182	189
$\sigma_\mathcal{R}(1/2)/\sigma_7(1/2)$	1	1.9996(3)	2.3327(5)	3.498(1)	3.997(2)	4.996(3)	5.991(5)	5.328(4)
$\sigma_\mathcal{R}(3/2)/\sigma_7(3/2)$	1	1.9989(7)	2.331(1)	3.495(5)	3.994(4)	4.989(7)	5.99(1)	5.321(9)
$\sigma_\mathcal{R}(5/2)/\sigma_7(5/2)$	1	1.996(1)	2.327(1)	3.484(5)	3.980(7)	4.96(1)	5.94(2)	5.29(1)
$\mathcal{C}'_\mathcal{R}$	1	2.0000	2.3333	3.5000	4.0000	5.0000	6.0000	5.3333

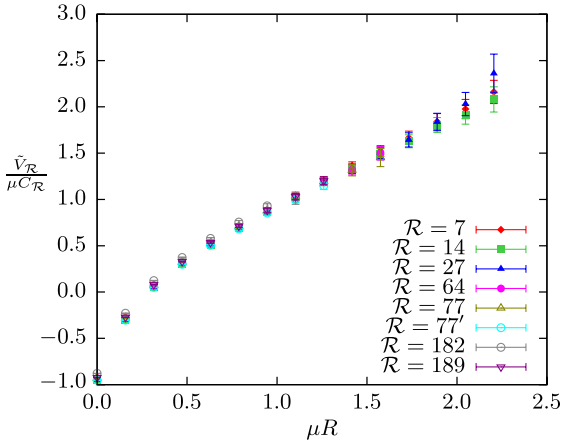

FIG. 5 (color online). Scaled potential with $\beta = 40$ on a 28^3 lattice.

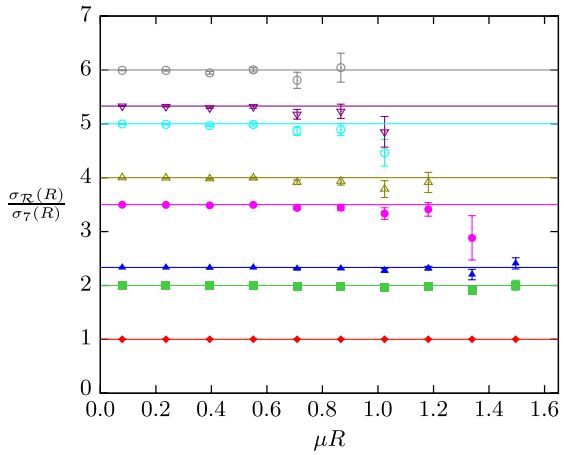

FIG. 6 (color online). Ratio of the local string tension with $\beta = 40$ scaled on a 28^3 lattice for the eight smallest representations.

B. Lüscher term

In Table IV we have seen that the dimensionless coefficient $\alpha_{\mathcal{R}}$ in the static potential scales with the quadratic Casimir, similarly to the string tension. The corresponding term, if measured at distances where the flux tube is fully developed, is referred to as the *Lüscher term*. Its value has been calculated by Lüscher for charges in the fundamental representation, in d dimensions $\alpha = (d-2)\pi/24$, and it is believed to be universal [51]. The value $\alpha = \pi/24$ in 3 dimensions is off the results in Table III. However, since the coefficients in this table are fitted to the static potential from $R = 1$ to values of R with acceptable signal to noise ratio, they contain contributions from the short range Coulombic tail. To calculate $\alpha_{\mathcal{R}}$ at intermediate distances we better use the (local) Lüscher term

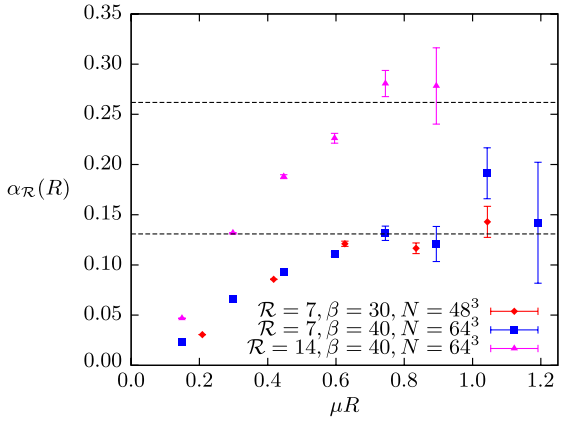

FIG. 7 (color online). Local Lüscher term at two different couplings and for two different representations.

$$\alpha_{\mathrm{loc},\mathcal{R}}(R) = \frac{\alpha_{\mathcal{R}} R^2}{R^2 - \rho^2} = \frac{R^3}{2\beta_T \rho^2} \times \ln \frac{\langle P_{\mathcal{R}}(0) P_{\mathcal{R}}(R+\rho)\rangle \langle P_{\mathcal{R}}(0) P_{\mathcal{R}}(R-\rho)\rangle}{\langle P_{\mathcal{R}}(0) P_{\mathcal{R}}(R)\rangle \langle P_{\mathcal{R}}(0) P_{\mathcal{R}}(R)\rangle}, \tag{50}$$

with $\rho = 1$. In Fig. 7 we plotted the local Lüscher term for charges in the 7 and 14 representation at couplings $\beta \in \{30, 40\}$. Our data for the defining 7 dimensional representation at intermediate distances are in agreement with the theoretical prediction $\alpha_7 = \pi/24 \approx 0.131$. The local Lüscher term for the adjoint representation approaches a value close to $\alpha_{14} \approx \pi/12$. Although this exceeds the universal prediction of [51] by a factor of 2 this behavior is in close analogy to the situation in 3 dimensional $SU(5)$ Yang-Mills theory where Casimir scaling of the local Lüscher term at short distances has been reported in [52] for the 10 dimensional representation. Since the Lüscher term is expected to show up at asymptotic large distances, this term can only be extracted if the flux tube has fully developed before string breaking sets in. Whether this is the case for G_2 gauge theory is not clear. Our results suggest that this happens for charges in the 7 dimensional representation.

C. String breaking and glue-lumps in 3 dimensions

To observe the breaking of strings connecting static charges at intermediate scales when one further increases the separation of the charges we performed high statistics LHMC simulations on a 48^3 lattice with $\beta = 30$. We calculated expectation values of Wilson loops and products of Polyakov loops for charges in the two fundamental representations of G_2. When a string breaks then each static charge in the representation $\mathcal{R}$ at the end of the string is screened by $N(\mathcal{R})$ gluons to form a color blind

glue lump. We expect that the dominant decay channel for an over-stretched string is string $\rightarrow$ glue lump + glue lump. For a string to decay the energy stored in the string must be sufficient to produce two glue lumps. According to (11) it requires at least 3 gluons to screen a static charge in the 7 representation, one gluon to screen a charge in the 14 representation and two gluons to screen a charge in the 27 representation. We shall calculate the separations of the charges where string breaking sets in and the masses of the produced glue lumps. The mass of such a quark-gluon bound state can be obtained from the correlation function according to

$$\exp(-m_{\mathcal{R}}T) \propto C_{\mathcal{R}}(T) = \left\langle \left(\bigotimes_{n=1}^{N(\mathcal{R})} F_{\mu\nu}(y) \right) \Big|_{\mathcal{R},a} \mathcal{R}(\mathcal{U}_{yx})_{ab} \left(\bigotimes_{n=1}^{N(\mathcal{R})} F_{\mu\nu}(x) \right) \Big|_{\mathcal{R},b} \right\rangle, \tag{51}$$

where $\mathcal{R}(\mathcal{U}_{yx})$ is the temporal parallel transporter in the representation $\mathcal{R}$ from x to y of length T. It represents the static sources in the representation $\mathcal{R}$. The vertical line means projection of the tensor product onto that linear subspace on which the irreducible representation $\mathcal{R}$ acts,

$$(14 \otimes 14 \otimes \cdots \otimes 14) = \mathcal{R} \oplus \ldots. \tag{52}$$

For example, for charges in the 14 representation the projection is simply

$$F_{\mu\nu}(x)|_{14,a} = F^a_{\mu\nu}(x), \quad \text{where } F^a_{\mu\nu}T^a = F_{\mu\nu}. \tag{53}$$

For charges in the 7 representation we must project the reducible representation $14 \otimes 14 \otimes 14$ onto the irreducible representation 7. Using the embedding of G_2 into $SO(7)$ representations one shows that this projection can be done with the help of the totally antisymmetric ε tensor with 7 indices,

$$F_{\mu\nu}(x) \otimes F_{\mu\nu}(x) \otimes F_{\mu\nu}(x)|_{7,a} \propto F^p_{\mu\nu}(x)F^q_{\mu\nu}(x)F^r_{\mu\nu}(x)\varepsilon_{abcdefg}T^p_{bc}T^q_{de}T^r_{fg}. \tag{54}$$

Figure 8 shows the logarithm of the glue-lump correlator (51) as function of the separation of the two lumps for static charges in the fundamental representations 7 and 14. The linear fits to the data yield the glue-lump masses

$$m_7 a = 0.46(4), \qquad m_{14} a = 0.761(3). \tag{55}$$

Thus, we expect that the subtracted static potentials approach the asymptotic values

$$\tilde{V}_{\mathcal{R}} \rightarrow 2m_{\mathcal{R}} - \gamma_{\mathcal{R}}. \tag{56}$$

With the fit values $\gamma_7 a = 0.197(1)$ and $\gamma_{14} a = 0.381(2)$ we find

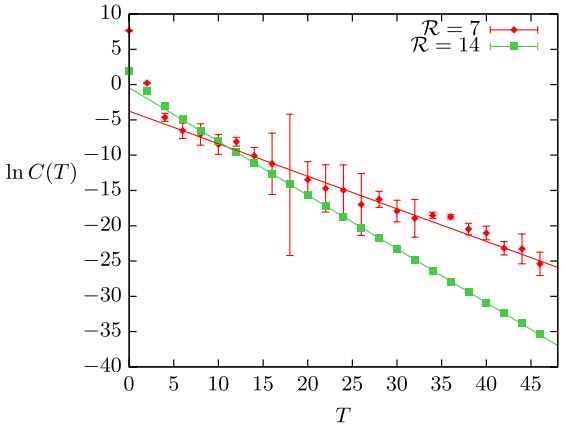

FIG. 8 (color online). Glue-lump correlator (lattice size 48^3, $\beta = 30$).

$$\tilde{V}_7/\mu \rightarrow 3.47, \qquad \tilde{V}_{14}/\mu \rightarrow 5.47. \tag{57}$$

Figure 9 shows the rescaled potentials for charges in the fundamental representations together with the asymptotic values (57) extracted from the glue-lump correlators. At fixed coupling $\beta = 30$ both potentials flatten exactly at separations of the charges where the energy stored in the flux tube is twice the glue-lump energy. However, the direct comparison of the potentials for two different couplings, i.e., different lattice spacings, reveals that the potential for adjoint charges is nearly free of lattice artifacts while the string breaking distance for charges in the defining representation is largely coupling dependent and the continuum limit is not reached yet.

A good approximation for the string breaking distance is then given by $V_{\mathcal{R}}(R^b) \approx 2m_{\mathcal{R}}$. Assuming Casimir scaling for the coefficients $\alpha_{\mathcal{R}}$, $\gamma_{\mathcal{R}}$, and $\sigma_{\mathcal{R}}$ in the static potential we obtain

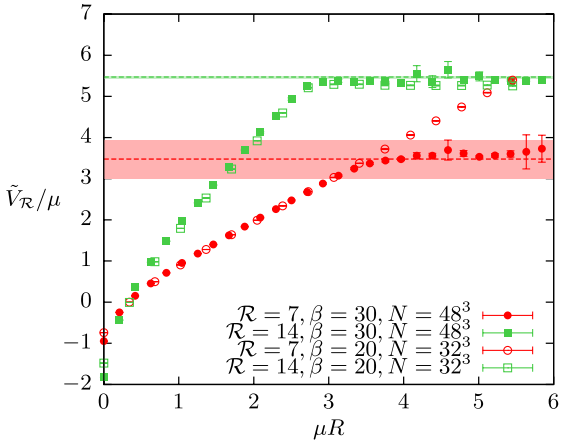

FIG. 9 (color online). Potential for both fundamental representations at $\beta \in \{20, 30\}$ and corresponding glue-lump mass for $\beta = 30$.

$$\mu R^b_{\mathcal{R}} = \left(\sqrt{\alpha_7 + \frac{1}{4}\left(\frac{\gamma_7}{\mu} - M_{\mathcal{R}}\right)^2} - \frac{1}{2}\left(\frac{\gamma_7}{\mu} - M_{\mathcal{R}}\right)\right),$$
$$M_{\mathcal{R}} = \frac{2m_{\mathcal{R}}}{\mu C'_{\mathcal{R}}}. \tag{58}$$

Inserting the result from the last row in Table III and the glue-lump masses we find $\mu R^b_7 = 3.49$ and $\mu R^b_{14} = 2.77$. These values agree well with the separations μR in Fig. 9 where the static potentials flatten such that string breaking sets in at scales predicted by formula (58). Figure 10 shows the local string tensions in the two fundamental representations and Fig. 11 their ratio. Especially the last plot makes clear that the string connecting charges in the adjoint representation break earlier than the string connecting charges in the 7 representation. Just at the critical separation predicted by formula (58) the ratio of local string tensions $\sigma_{14}(R)/\sigma_7(R)$ shows indeed a pronounced knee.

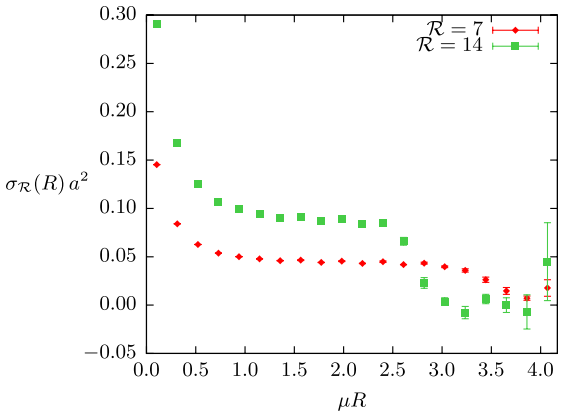

FIG. 10 (color online). Local string tension (48^3 lattice, $\beta = 30$).

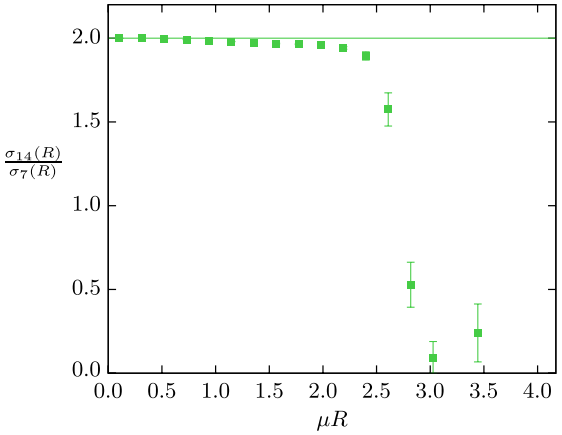

FIG. 11 (color online). Casimir scaling of local string tension (48^3 lattice, $\beta = 30$).

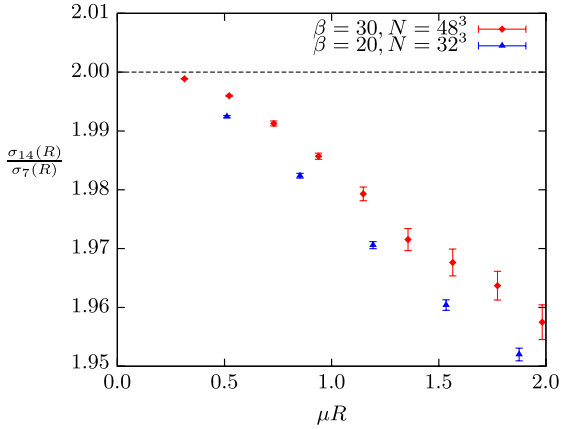

FIG. 12 (color online). Deviations from Casimir scaling at two different couplings.

D. Signs of Casimir scaling violations

Although the coarse grained view onto the ratio of local string tensions up to the string breaking distance (Fig. 11) shows an approximate Casimir scaling, a closer look uncovers deviations from the expected Casimir ratio of the adjoint and defining representation (see Fig. 12). The results for two different lattice spacings indicate that for short distances, in the Coulombic part of the potential, Casimir scaling is fulfilled, in agreement with the predictions of perturbation theory, valid at short distances. For larger distances the measured ratio drops by about 2.5% near the string breaking distance and similar deviations have already been reported in [36,39] in 3 dimensional $SU(2)$ gauge theory. In either case the scale dependence identifies Casimir scaling violations as a purely nonperturbative long range effect. Of course, the given error bounds in Fig. 12 may be taken with care as they include only statistical uncertainties. Lattice artifacts are still visible and further work will be necessary to confirm that this violation persists in the continuum limit.

E. Continuum limit of the string tension

Equation (16) gives the string tension in the continuum as a function of the coupling $\beta \propto 1/g^2$ [20]. To compare this continuum result with our lattice data we extrapolate the corresponding value $g^{-2}\sqrt{\sigma_7}$ linearly in $\beta^{-1} \propto a$ to the

TABLE VI. String tension for the 7 representation on lattice sizes and couplings that are used for the continuum extrapolation.

β	N	$\sigma_7 a^2$	$g^{-2}\sqrt{\sigma_7}$
20	32^3	0.118 07(19)	0.4908(4)
25	40^3	0.068 63(12)	0.4678(4)
30	48^3	0.044 81(28)	0.4536(14)
35	56^3	0.031 93(14)	0.4467(10)
40	64^3	0.022 19(33)	0.4256(32)

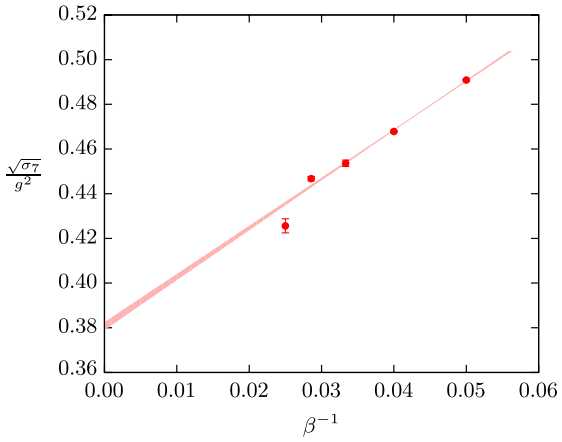

FIG. 13 (color online). Linear continuum extrapolation of the string tension. The shaded region indicates the corresponding error bound.

continuum limit by using the couplings and lattice sizes in Table VI. This procedure is motivated by the (in leading order) linear behavior that has been found in a similar study for gauge groups $SU(2)$ up to $SU(5)$ [53]. For increasing β the scaling window with a linear rising potential shrinks and it becomes more difficult to extract reliable values for the intermediate string tension. Thus, a linear fit to all points in Table VI leads to $g^{-2}\sqrt{\sigma_7} = 0.381(5)$ (see Fig. 13) with a rather large reduced $\chi^2 = 8.56$, whereas a linear fit to the reliable data points with the 3 smallest β values yields $g^{-2}\sqrt{\sigma_7} = 0.376(2)$ with a small reduced $\chi^2 = 0.51$. Both fit values are in good agreement with the prediction of Eq. (16), $g^{-2}\sqrt{\sigma_7} = 0.398\,94$.

Corrections to this theoretical value have been derived in a systematic expansion in [21]

$$g^{-2}\sqrt{\sigma_7} = \sqrt{\frac{1}{2\pi}}(1 - 0.027\,99 + \cdots) \approx 0.387\,78, \quad (59)$$

but they are still subject to ambiguities in defining a low momentum cutoff that may change this value by up to 3%. Keeping in mind that we are left with possible systematic uncertainties in the extrapolation procedure that are not reflected in the given statistical error a complete agreement between analytical and numerical results is apparent.

F. Casimir scaling in 4 dimensions

In this last section we present our results for the static potential in 4 dimensions. The LHMC simulations have been performed on a small 14^4 and a larger 20^4 lattice for different values of β. The static potentials and local string tensions have been extracted from (43) and (46), where the expectation values have been calculated with a two-step Lüscher-Weisz algorithm. Table VII contains the fits to the parameters in the potential for static charges in the 7 representation for these lattices and values for β.

TABLE VII. Parameters of the quark antiquark potential in 4 dimensions for $\mathcal{R} = 7$.

	$\beta = 9.7$, $N = 14^4$	$\beta = 10$, $N = 14^4$	$\beta = 9.7$, $N = 20^4$
$\gamma_7 a$	0.83(8)	0.74(4)	0.68(9)
α_7	0.40(7)	0.33(3)	0.28(8)
$\sigma_7 a^2$	0.07(2)	0.042(9)	0.11(1)

Figure 14 shows the static potentials in "physical units" $\mu = \sqrt{\sigma_7}$ for charges in the 7, 14, 27, and 64 dimensional representations and coupling $\beta = 9.7$ as a function of the distance between the charges in physical units. The corresponding value for σ_7 is taken from Table VII. The same coupling has been used in [16] on an asymmetric $14^3 \times 28$ lattice. After normalizing the potential with the quadratic Casimirs they are identical within error bars, as can be seen in Fig. 15. Our findings are in complete agreement with the

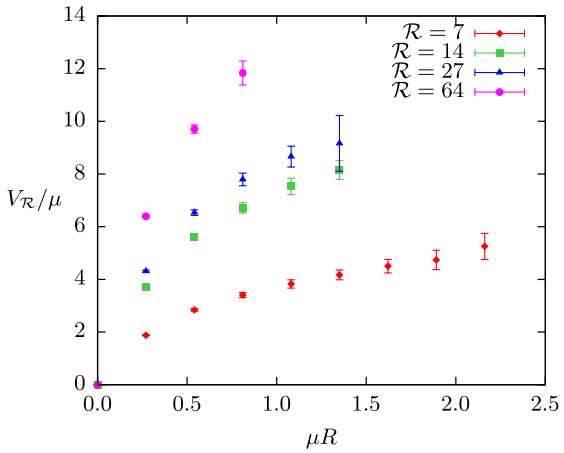

FIG. 14 (color online). Unscaled potential at $\beta = 9.7$ on a 14^4 lattice.

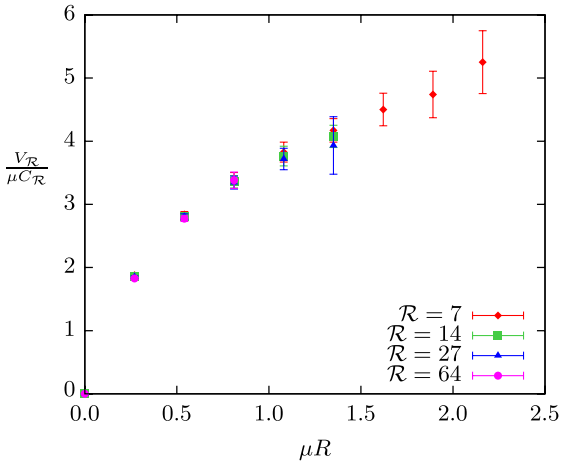

FIG. 15 (color online). Scaled potential at $\beta = 9.7$ on a 14^4 lattice.

results in [16] on Casimir scaling in 4 dimensional G_2 gluodynamics at $\beta = 9.7$ and our accurate results on Casimir scaling on intermediate scales in 3 dimensional G_2 gluodynamics.

Figures 16 and 17 show the corresponding results for a weaker coupling $\beta = 10$ closer to the continuum limit. For this small coupling we can measure the potential only up to separations $\mu R \approx 1.5$ of the charges. But we can do this with high precision and for higher-dimensional representations. As for $\beta = 9.7$ we find that the potentials normalized with the second order Casimirs fall on top of each other. This confirms Casimir scaling for G_2 gluodynamics in 4 dimensions for charges in representations with dimensions 7, 14, 27, 64, 77, 77′, 182, and 189.

Finally, we simulated on a much larger 20^4 lattice at $\beta = 9.7$ in order to calculate the static potential for larger separations of the static quarks. Unfortunately the distance $\mu R \approx 3$ is still not sufficient to detect string breaking, see Fig. 18. But again the potentials normalized with the quadratic Casimirs shown in Fig. 19 are equal within error bars.

In Table VIII we have listed the fit values for the parameters of the potentials on the larger 20^4 lattice for static charges in the representations with dimensions 7, 14, and 27. For all representation we find Casimir scaling of all three parameters in the potential. Unfortunately the fit parameters cannot be determined reliably in the 64 representation with the present data. This is attributed to larger errors for the potentials at intermediate scales, see Fig. 18, so that the parameters can only be determined from the ultraviolet part of the potential for this representation ($R < 3$) which is rather Coulomb-like than linearly rising. Much more conclusive are the local string tensions calculated on the larger lattice (now up to the 64 representation). Table IX contains the local string tensions divided by the

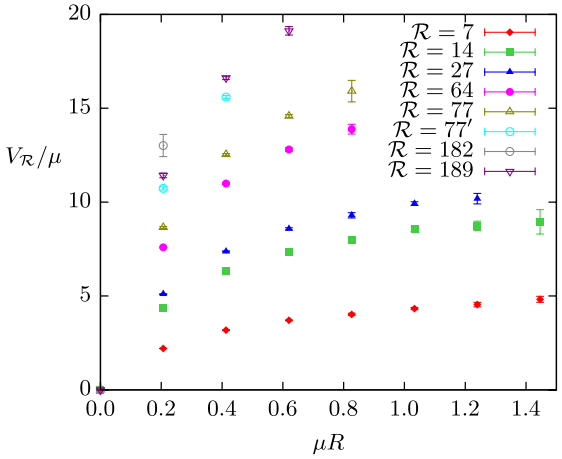

FIG. 16 (color online). Unscaled potential at $\beta = 10$ on a 14^4 lattice.

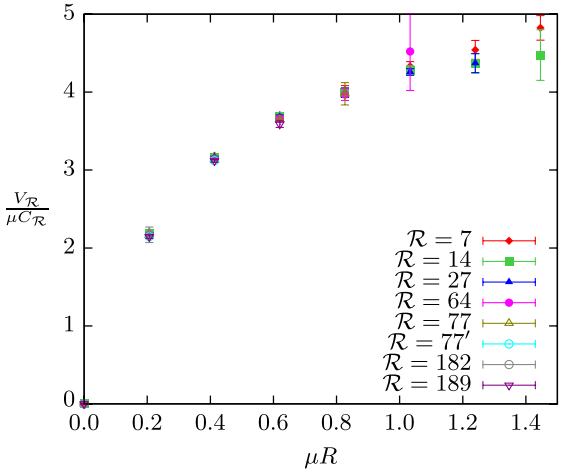

FIG. 17 (color online). Scaled potential at $\beta = 10$ on a 14^4 lattice.

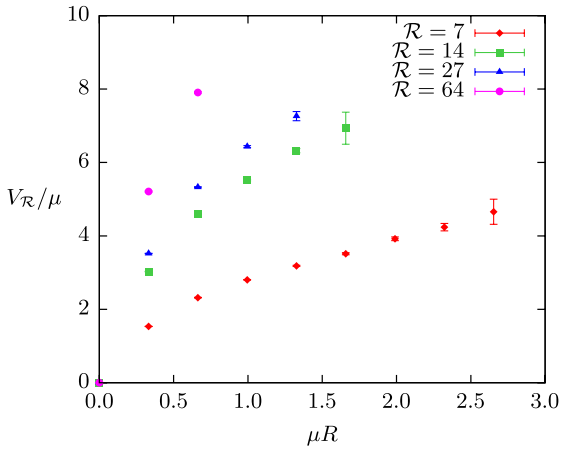

FIG. 18 (color online). Unscaled potential at $\beta = 9.7$ on a 20^4 lattice.

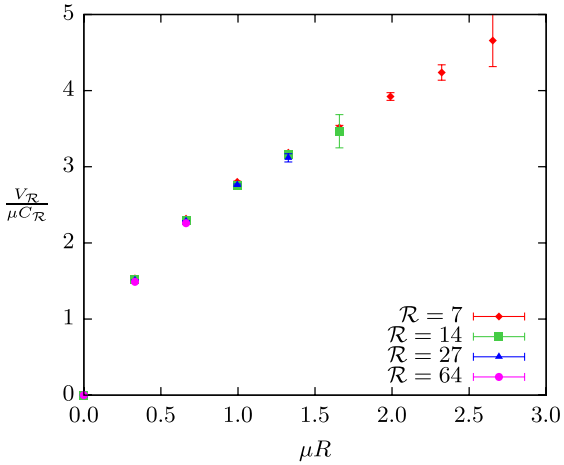

FIG. 19 (color online). Scaled potential at $\beta = 9.7$ on a 20^4 lattice.

TABLE VIII. Fit parameters of static potentials (20^4 lattice, $\beta = 9.7$).

$\mathcal{R}$	7	14	27
$\gamma_{\mathcal{R}} a$	0.68(9)	1.39(4)	1.61(3)
$\gamma_{\mathcal{R}} a/C'_{\mathcal{R}}$	0.68	0.695	0.690
$\alpha_{\mathcal{R}}$	0.28(8)	0.60(2)	0.69(2)
$\alpha_{\mathcal{R}}/C'_{\mathcal{R}}$	0.28	0.30	0.295
$\sigma_{\mathcal{R}} a^2$	0.11(1)	0.21(1)	0.251(9)
$\sigma_{\mathcal{R}} a^2/C'_{\mathcal{R}}$	0.11	0.105	0.107

TABLE IX. Scaled local string tension (20^4 lattice, $\beta = 9.7$).

$\mathcal{R}$	7	14	27	64
$\sigma_{\mathcal{R}}(1/2)/\sigma_7(1/2)$	1	1.973(1)	2.294(1)	3.396(8)
$\sigma_{\mathcal{R}}(3/2)/\sigma_7(3/2)$	1	1.987(3)	2.303(4)	3.44(2)
$\sigma_{\mathcal{R}}(5/2)/\sigma_7(5/2)$	1	1.92(1)	2.28(3)	-
$C'_{\mathcal{R}}$	1	2.0000	2.3333	3.5000

local string tensions in the 7 representation. These normalized values are constant up to separations of the charges where the statistical errors are under control. Compared to the corresponding numbers in 3 dimensions, see Table V, we now see a slight dependence of the local string tensions from Eq. (59) on the distance R. Despite of the lower precision of the results in 4 dimensions compared to the corresponding results in 3 dimensions we again confirm Casimir scaling on short to intermediate scales within 5%.

All our simulation results for the local string tensions $\sigma_{\mathcal{R}}(R)$ normalized by $\sigma_7(R)$ on a 14^4 lattice with $\beta \in \{9.7, 10\}$ and on a 20^4 lattice with $\beta = 9.7$ and for $\mu R \leq 1.5$ are collected in Fig. 20. The horizontal lines in this figure show the prediction of the Casimir scaling hypothesis. The normalized data points are compatible with each other and with the hypothesis.

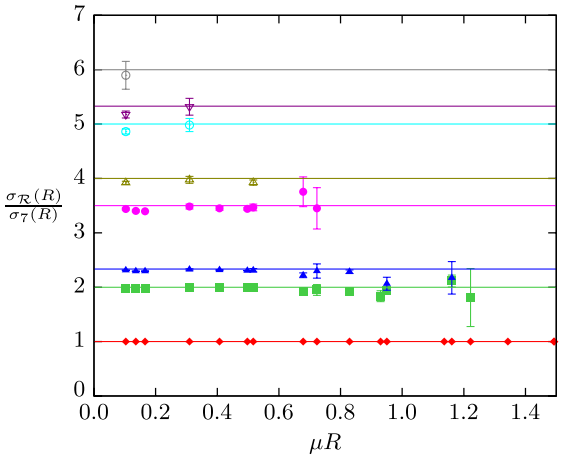

FIG. 20 (color online). Scaled local string tension with $\beta \in \{9.7, 10\}$ on 14^4 and 20^4 lattices.

VI. CONCLUSIONS

In the present work we implemented an efficient and fast LHMC algorithm to simulate G_2 gauge theory in three and four dimensions. With only a slight modification we can include a (normalized) Higgs field in the 7 representation. The corresponding results for the phase diagram of G_2 Yang-Mills–Higgs theory will soon be presented in a companion paper. The algorithm has been optimized with the help of the coset decomposition of group elements and the analytic expressions for the exponential maps for the two factors. In addition we implemented a slightly modified Lüscher-Weisz multistep algorithm with exponential error reduction to measure the static potentials for charges in various G_2 representations. The accurate results in 3 dimensions show that all parameters of the fitted static potentials show Casimir scaling, see Table III. The global string tensions extracted from these fits show that possible deviations from Casimir scaling must be less than 4%. We also extracted the local string tensions from the Creutz ratios to obtain even more precise data. This way we confirm Casimir scaling at short distances $\sqrt{\sigma_7} R < 1$ with 1% accuracy. Thus we conclude that in 3 dimensional G_2 gluodynamics the Casimir scaling violations of the string tensions are small for all charges in the representations with dimensions 7, 14, 27, 64, 77, 77′, 182, and 189.

For charges in the two fundamental representations we performed LHMC simulations on larger lattices to detect string breaking at asymptotic scales. In 3 dimensions we observe that string breaking indeed sets in at the expected scale where the energy stored in the flux tube is sufficient to create two glue lumps. To confirm this expectation we calculated masses of glue lumps associated with static charges in the fundamental representations. Here, close to the string breaking distance, systematic Casimir scaling violations show up at the 2.5% level and they are identified as a nonperturbative effect arising only at large distances. Finally, the prediction for the numerical value of the string tension in 3 dimensions is confirmed by a continuum extrapolation of our precise data.

In 4 dimensional G_2 gluodynamics we found Casimir scaling for charges in the representations 7, 14, 27, and 64, similarly as we did in 3 dimensions, although the uncertainties are of course larger. But within error bars we see no violation of Casimir scaling and this confirms the corresponding results in [16], obtained with a variant of the smearing procedure. To see the expected string breaking in 4 dimensions one would need larger lattices than those used in the present work.

ACKNOWLEDGMENTS

Helpful discussions with Philippe de Forcrand, Christof Gattringer, Kurt Langfeld, and Uwe-Jens Wiese are gratefully acknowledged. C. Wozar thanks for the support by the Studienstiftung des deutschen Volkes. This work has been supported by the DFG under GRK 1523.

[1] B. Svetitsky and L. G. Yaffe, Nucl. Phys. **B210**, 423 (1982).
[2] L. G. Yaffe and B. Svetitsky, Phys. Rev. D **26**, 963 (1982).
[3] C. Wozar, T. Kästner, A. Wipf, T. Heinzl, and B. Pozsgay, Phys. Rev. D **74**, 114501 (2006).
[4] B. Wellegehausen, A. Wipf, and C. Wozar, Phys. Rev. D **80**, 065028 (2009).
[5] A. Wipf, T. Kaestner, C. Wozar, and T. Heinzl, SIGMAP bulletin **3**, 006 (2007).
[6] C. Gattringer, Phys. Rev. Lett. **97**, 032003 (2006).
[7] F. Synatschke, A. Wipf, and C. Wozar, Phys. Rev. D **75**, 114003 (2007).
[8] E. Bilgici, F. Bruckmann, C. Gattringer, and C. Hagen, Phys. Rev. D **77**, 094007 (2008).
[9] J. Kogut, J. Polonyi, H. Wyld, and D. Sinclair, Phys. Rev. Lett. **54**, 1980 (1985).
[10] F. Karsch and M. Lütgemeier, Nucl. Phys. **B550**, 449 (1999).
[11] P. Forcrand and O. Jahn, Nucl. Phys. **B651**, 125 (2003).
[12] C. Ford, T. Tok, and A. Wipf, Nucl. Phys. **B548**, 585 (1999).
[13] M. Pepe and U. J. Wiese, Nucl. Phys. **B768**, 21 (2007).
[14] K. Holland and M. Pepe, and U. J. Wiese, Nucl. Phys. **B694**, 35 (2004).
[15] K. Holland, P. Minkowski, M. Pepe, and U. J. Wiese, Nucl. Phys. **B668**, 207 (2003).
[16] L. Liptak and S. Olejnik, Phys. Rev. D **78**, 074501 (2008).
[17] J. Greensite, Prog. Part. Nucl. Phys. **51**, 1 (2003).
[18] A. J. Macfarlane, Int. J. Mod. Phys. A **17**, 2595 (2002).
[19] J. Ambjorn, P. Oleson, and C. Peterson, Nucl. Phys. **B240**, 533 (1984).
[20] D. Karabali, C. j. Kim, and V. P. Nair, Nucl. Phys. **B524**, 661 (1998).
[21] D. Karabali, V. P. Nair, and A. Yelnikov, Nucl. Phys. **B824**, 387 (2010).
[22] Yu. A. Simonov, arXiv:1003.3608.
[23] G. I. Poulis and H. D. Trottier, Phys. Lett. B **400**, 358 (1997).
[24] J. Ambjorn, P. Oleson, and C. Peterson, Nucl. Phys. **B240**, 189 (1984).
[25] C. Michael, Nucl. Phys. **259**, 58 (1985).
[26] L. A. Griffiths, C. Michael, and P. E. L. Rakov, Phys. Lett. **150B**, 196 (1985).
[27] H. D. Trottier, Phys. Lett. B **357**, 193 (1995).
[28] M. Müller, W. Beirl, M. Faber, and H. Markum, Nucl. Phys. B, Proc. Suppl. **26**, 423 (1992).
[29] N. A. Campbell, I. H. Jorysz, and C. Michael, Phys. Lett. **167B**, 91 (1986).
[30] C. Michael, Nucl. Phys. B, Proc. Suppl. **26**, 417 (1992).
[31] G. Bali, Phys. Rev. D **62**, 114503 (2000).
[32] C. Piccioni, Phys. Rev. D **73**, 114509 (2006).
[33] O. Philipsen and H. Wittig, Phys. Lett. B **451**, 146 (1999).
[34] P. W. Stephenson, Nucl. Phys. **B550**, 427 (1999).
[35] P. de Forcrand and O. Phillipsen, Phys. Lett. B **475**, 280 (2000).
[36] S. Kratochvila and P. de Forcrand, Nucl. Phys. **B671**, 103 (2003).
[37] L. Del Debbio, H. Panagopoulos, P. Rossi, and E. Vicari, Phys. Rev. D **65**, 021501 (2001).
[38] B. Lucini and M. Teper, Phys. Rev. D **64**, 105019 (2001).
[39] S. Kratochvila and P. de Forcrand, Nucl. Phys. B, Proc. Suppl. **119**, 670 (2003).
[40] M. Pepe and U.-J. Wiese, Phys. Rev. Lett. **102**, 191601 (2009).
[41] O. Philipsen and H. Wittig, Phys. Rev. Lett. **81**, 4056 (1998).
[42] H. D. Trottier, Phys. Rev. D **60**, 034506 (1999).
[43] H. D. Trottier and K. Y. Wong, Phys. Rev. D **72**, 054505 (2005).
[44] C. DeTar, O. Kaczmarek, K. Karsch, and E. Laermann, Phys. Rev. D **59**, 031501 (1998).
[45] G. Bali, H. Neff, T. Düssel, T. Lippert, and K. Schilling, Phys. Rev. D **71**, 114513 (2005).
[46] J. Greensite, K. Langfeld, S. Olejnik, H. Reinhardt, and T. Tok, Phys. Rev. D **75**, 034501 (2007).
[47] P. Marenzoni, L. Pugnetti, and P. Rossi, Phys. Lett. B **315**, 152 (1993).
[48] B. Gehrmann and U. Wolff, Nucl. Phys. B, Proc. Suppl. **83-84**, 801 (2000).
[49] A. Laufer, J. Phys. A **30**, 5455 (1997).
[50] M. Luescher and P. Weisz, J. High Energy Phys. 09 (2001) 010.
[51] M. Lüscher, Nucl. Phys. **B180**, 317 (1981).
[52] H. B. Meyer, Nucl. Phys. **B758**, 204 (2006).
[53] M. J. Teper, Phys. Rev. D **59**, 014512 (1998).